Cellular and Molecular Life Sciences (2026) 83:41
https://doi.org/10.1007/s00018-025-06023-x

ORIGINAL ARTICLE

Bone marrow mesenchymal stem cell-derived circHECTD1 targets claudin1 through the CTCF/METTL3 axis to alleviate ulcerative colitis

Short title: BMSC-derived circHECTD1 alleviates UC

Kailing Wang[1] · Fan Liu[1] · Jiawen Deng[1] · Jing Peng[1] · Miao Wang[1] · Houxiang Zhou[1] · Yan Xu[2] · Fujun Li[1] · Miao Ouyang[1,3,4]

Received: 14 April 2025 / Revised: 26 November 2025 / Accepted: 8 December 2025

Abstract

Objective Ulcerative colitis (UC) is an inflammatory bowel disease that lacks satisfactory treatment. This study aimed to investigate the role of bone marrow mesenchymal stem cell-derived exosomal circHECTD1 (Exo-circHECTD1) in UC and its mechanism of action.

Methods An inflammatory model was created using LPS-stimulated MODE-K cells and an UC mouse model was established using dextran sodium sulfate (DSS). Cell proliferation was assessed using CCK-8. Apoptosis and Th17/Treg cell differentiation were analyzed by flow cytometry. Inflammatory factors were detected using ELISA. FITC fluorescence intensity was measured to evaluate permeability. m^6A modification and molecular binding were detected using immunoprecipitation methods. Luciferase reporters were used to evaluate METTL3 promoter activity. RT-qPCR was used to detect RNA expression and western blotting was used to detect METTL3, CTCF, claudin1, and tight junction proteins (ZO-1, occludin).

Results Exo-circHECTD1 enhanced viability and permeability and reduced apoptosis and inflammation factor levels in LPS-treated MODE-K cells. Moreover, it reduced the Th17/Treg ratio, regulated gut microbiota, and promoted the recovery of mice with DSS-induced UC. Claudin1 knockdown reversed the protective effect of Exo-circHECTD1 on UC models. CircHECTD1 binds to CTCF, which binds to the METTL3 promoter and promotes METTL3 promoter activity. METTL3 upregulates the level of claudin1 m^6A modification and inhibits claudin1 expression. CTCF or METTL3 knockdown alleviated LPS-induced MODE-K cell damage.

Conclusion Exo-circHECTD1 inhibits METTL3 transcription by binding to CTCF to reduce claudin1 m^6A modification and promote claudin1 expression, thereby regulating the balance of gut microbiota and Th17/Treg cells and alleviating UC.

Keywords Ulcerative colitis · Exo-circHECTD1 · Claudin1 · M^6A modification · Th17/Treg cell balance

Kailing Wang and Fan Liu These authors are regarded as co-first authors.

✉ Yan Xu
YeshuaChristille@163.com

✉ Fujun Li
CurtisDavis@163.com

✉ Miao Ouyang
oym3399@csu.edu.cn

[1] Department of Gastroenterology, Xiangya Hospital, Central South University, No. 87, Xiangya Road, Kaifu District, Changsha 410008, Hunan, China

[2] Department of Health Management Center, Xiangya Hospital, Central South University, No. 87, Xiangya Road, Kaifu District, Changsha 410008, Hunan, China

[3] National Clinical Research Center for Geriatric Disorders, Xiangya Hospital, Central South University, Changsha 410008, Hunan, China

[4] Department of Gastroenterology, National Clinical Research Center for Geriatric Disorders, Xiangya Hospital, Central South University, No. 87, Xiangya Road, Kaifu District, Changsha 410008, Hunan, China

Published online: 26 December 2025

Introduction

Ulcerative colitis (UC) is a lifelong inflammatory bowel disease that is increasing in incidence worldwide [1]. It is hypothesized to be associated with exposures to environmental risk factors leading to an improper immune response to the gut microbiota in genetically predisposed individuals and is usually manifested by bloody diarrhoea, abdominal pain, and fecal incontinence [2, 3]. Currently, a wide variety of drugs, including mesalamine, glucocorticoids, azathioprine, biological agents, JAK inhibitors, and calcineurin inhibitors, are available for the treatment of UC [4]. However, the rapidly expanding range of treatment options has urged a need for personalized medicine to achieve optimal disease control [5]. A better understanding of the biological mechanisms driving UC may improve medical decisions and support the development of novel drugs.

Colonic mucus barrier damage is a common and key pathogenic event in UC [6]. This physical barrier is formed by mucus secreted from goblet cells in the intestinal epithelium to allow passage of small molecules and hinder translocation of microorganisms, thereby protecting the epithelium [7]. Tight junctions between epithelial cells are important regulators of such transepithelial permeability [8]. Claudin1 is a tight junction protein that maintains intestinal epithelial barrier function [9]. Claudin1 expression is decreased in UC [10, 11]. Therefore, claudin1 can be targeted to improve intestinal barrier function and alleviate UC.

In recent years, mesenchymal stem cell (MSC)-derived exosomes have demonstrated great potential to manage various diseases at both preclinical and clinical levels [12]. Exosomes can impose phenotypic and molecular alterations on recipient cells by delivering their cargo of proteins, lipids, metabolites, and nucleic acids (DNA, mRNA, and noncoding RNAs) [13]. Circular RNAs (circRNAs) are a group of single-stranded closed noncoding RNAs that have been recognized as important regulators of gene expression in a variety of diseases [14]. However, the role of circRNAs in UC has been insufficiently studied. We have previously detected downregulation of circHECTD1 expression in colonic mucosal tissues of patients with UC and further discovered that circHECTD1 overexpression can reduce colonic injury and inflammation in mice with DSS-induced UC by upregulating the expression of the pro-autophagic protein HuR via targeted inhibition of miR-182-5p [15]. Therefore, circHECTD1 may be delivered using exosomes to target dysregulated factors such as claudin1 in the intestinal epithelium, thereby alleviating UC.

This study aimed to determine whether exosomal circHECTD1 can alleviate UC by targeting claudin1 and also uncover the mechanism by which circHECTD1 regulates claudin1, providing novel insights into the pathogenesis of UC and a theoretical basis for exosome treatment of this disease.

Materials and methods

Bone marrow MSC (BMSC) isolation and culture

BALB/c mice (Hunan SJA Laboratory Animal Co., Ltd., Changsha, Hunan, China) were used for experiments under the approval of the Animal Ethics Committee of Xiangya Hospital, Central South University. Animals were sacrificed by cervical dislocation after ether anesthesia, followed by the removal of tibiae and femora on a sterile operating table. The epiphyses on both sides of the bone were cut off and the bone marrow was flushed out with BMSC culture media (RASMX-90011, Cyagen, Guangzhou, China). Cells were disaggregated by pipetting. The single cell suspension was poured through a cell filter (70 μm) and spun at 1200 rpm for 5 min to remove the fat layer and lymphocytes. The cell pellet was washed thrice with PBS, resuspended in BMSC culture media, and cultured at 37 °C with 5% CO_2. After 24 h, the media were changed and non-adherent cells were discarded. Thereafter the media were changed every 3 days. Cells were passaged at a density of 1:2. Cells at passage 3 were used for experiments.

Cell identification by flow cytometry

BMSCs were incubated with CD105 (1:1000, ab2529, Abcam, Cambridge, UK), CD90 (1:2000, ab307736, Abcam), CD45 (1:2000, ab40763, Abcam), CD31 (1:2000, ab9498, Abcam), or CD29 (1:500, ab30394, Abcam) antibodies or corresponding isotype control antibodies for 25 min and analyzed by flow cytometry.

Osteogenic/adipogenic differentiation

Culture media were replaced to induce adipogenic or osteogenic differentiation of third-generation BMSCs in the logarithmic growth phase. These cells were stained with Oil Red O (Sigma, USA) or Alizarin Red (Sigma) to observe adipogenic or osteogenic differentiation, respectively.

Exosome isolation and identification

Third-generation BMSCs (80% confluent) were cultured in exosome-free media consisting of DMEM/F-12 and 10% exosome-free FBS (Gibco, USA). After 24 h of cell incubation, the supernatant was collected and centrifuged (300 × *g*, 10 min; 2000 × *g*, 10 min; 10000 × *g*, 30 min; 100000 × *g*, 70 min, twice). The precipitate was resuspended in PBS. Exosomes were observed using a transmission electron

microscope (Hitachi, Japan). The diameter of exosomes was measured and analyzed using ZetaView (Particle Metrix, Germany). The expression of calnexin, CD63, HSP70, and TSG101 was detected by western blotting.

Exosome uptake detection by immunofluorescence

MODE-K cells were seeded at a density of 2×10^4 cells per well into a 24-well plate and cultured for 24 h. Then the cells were cultured with PKH26 (Sigma)-labeled exosomes (100 μg/mL) for 24 h. After fixation with 4% paraformaldehyde, the cells were stained with DAPI (Beyotime, China) and observed under a microscope (Zeiss, Germany).

Cell culture and transfection

Mouse intestinal epithelial MODE-K cells (iCell, China) were cultured in 10% FBS-containing DMEM (Gibco). Knockdown vectors (sh-CTCF, sh-METTL3, and sh-claudin1), overexpression vectors (OE-claudin1), and negative control vectors (OE-NC and sh-NC) were purchased from RiboBio (Guangzhou, China) and transfected into MODE-K cells using a RiboFECT™ CP transfection kit (RiboBio). The transfection efficiency was determined after 48 h. Successfully transfected cells were incubated with 1 μg/mL LPS (Sigma) for 24 h and then with exosomes or Exo-circHECTD1 for 24 h before other experiments.

CCK-8 viability assay

Cells were transferred to a 96-well plate (5×10^4 cells/well) and maintained for 48 h. Then the cells were incubated with 10 μL/well CCK-8 reagent at 37 °C in the dark for 2 h. Optical density at 450 nm ($OD_{450\ nm}$) was determined using a microplate reader (Thermo Fisher Scientific, USA) to assess cell viability.

Apoptosis analysis

Cells were harvested at 80% confluence and 1×10^6 cells were washed twice with prechilled PBS. Then the cells were suspended in 1X Annexin buffer, incubated with 5 μL of Annexin V-FITC (88-8005-74, eBioscience, New York, USA) at room temperature for 10 min away from light, suspended in 300 μL of 1X Annexin buffer after a wash with precooled PBS, and injected into a flow cytometer (Guava® easyCyte 12, Millipore, USA) to measure apoptosis.

ELISA to detect inflammatory factors

Cell culture media or retroorbital blood of mice was centrifuged and the supernatant was collected for the detection of IL-1β (PI301, Beyotime) and TNF-α (PT512, Beyotime). Sandwich enzyme immunoassay technique was utilized and $OD_{450\ nm}$ was measured. According to the absorbance values of the serially diluted cytokine standard, a standard curve was drawn to calculate the sample concentration.

Permeability assay

Monolayer MODE-K cells seeded in transwell chambers were incubated with FITC-Dextran 4 kDa (FD4; 60842-46−8, Sigma-Aldrich, USA) for 2 h. The fluorescein intensity of the medium in the lower chamber was determined to analyze cell membrane permeability. FD4 was administered by gavage to animals ($n = 8$/group) at 400 μg/g. Intestinal permeability was evaluated by quantifying FITC fluorescence in plasma.

UC mouse model establishment

All animal experiments were authorized by the Ethics Committee of Xiangya Hospital, Central South University and were carried out in strict accordance with the *Guidelines for the Ethical Review of Laboratory Animal Welfare* in China. Male specific pathogen-free (SPF) C57BL/6 and BALB/c mice (4 weeks, 15–17 g, Hunan SJA Laboratory Animal Co., Ltd.) were housed in an SPF environment. Mice were given an enema of 1×10^{12} vg/mL AAV-sh-claudin1 (RiboBio) to inhibit claudin1 expression and the dextran sulfate sodium (DSS)-induced UC model was established 4 weeks later. DSS (3% m/v, MP Biomedicals, CA, USA) in water was administered for 7 consecutive days. Starting from 1 day before modeling, mice in the DSS-Exo group were intraperitoneally injected with 50 μg of exosomes every other day and mice in the sham and DSS groups were intraperitoneally injected with PBS (control). During the entire experimental period, the survival rate, general condition, body weight, diarrhoea, and blood in stool of the animals were monitored daily and the disease activity index (DAI; Table 1) of each mouse was recorded daily according to the standard protocol. The mice in each group were euthanatized by cervical dislocation on the 8th day and colon tissues were collected. If the animal died prematurely, affecting the collection of histological data, it was excluded.

Histological examination

Colon tissues were fixed with 4% paraformaldehyde, embedded in paraffin, cut into 5-μm sections, attached to

Table 1 Criteria for disease activity index

Loss of weight (%)	Stool consistency	Bloody stool	Score
0	Normal	Normal	0
1-5	/	/	1
6-10	Loose	Occult bleeding	2
10-15	/	/	3
>15	Diarrhea	Gross bleeding	4

Table 2 Histological scores

Score	Inflammation	Mucosal damage	Regeneration	Crypt damage	Range of lesions
0	None	None	Complete regeneration or normal tissue	None	0%
1	Mild	Mucous layer	Almost complete regeneration	Basal 1/3 damage	1%–25%
2	Moderate	Mucousa and submucosa	Regeneration with crypt depletion	Basal 2/3 damage	26%–50%
3	Severe	Transmural	Surface epithelium not intact	Crypt lost; surface epithelium present	51%–75%
4	-	-	No tissue repair	Crypt and surface epithelium lost	76%–100%

slides, and then dyed with hematoxylin and eosin. The slides were scanned using a Pannoramic MIDI scanner (3DHISTECH Ltd., Budapest, Hungary) and viewed using Pannoramic Viewer 1.15.4 (3DHISTECH Ltd.). Histopathological changes were evaluated according to a previously developed scoring system [16] (Table 2).

Microbiome analysis

DNA was extracted from mouse feces using a DNeasy PowerSoil kit (Qiagen) and quantified using Quant-iT PicoGreen (Invitrogen). DNA amplification was performed using a universal primer pair with Illumina adapter overhang sequences (V3 forward primer: 5'-TCG TCG GCA GCG TCA GAT GTG TAT AAG AGA CAG CCT ACG GGN GGC WGC AG-3'; V4 reverse primer: 5'-GTC TCG TGG GCT CGG AGA TGT GTA TAA GAG ACA GGA CTA CHV GGG TAT CTA ATCC-3'). PCR products were quantified using a KAPA Library Quantification kit (KAPA Biosystems Inc.) and TapeStation D1000 ScreenTape (Agilent Technologies). Paired-end sequencing was conducted by Macrogen using the MiSeq™ platform (Illumina) to cluster operational taxonomic units for diversity analysis.

Flow cytometry to determine the ratio of T-helper (Th)17/regulatory T (Treg) cells

For Th17 cell staining, mesenteric lymph nodes and lamina propria lymphocytes were stimulated with phorbol 12-myristate-13-acetate (100 ng/mL), ionomycin (1 mg/mL), and brefeldin A (10 mg/mL) at 37 °C for 5 h. After blocking with anti-CD16+CD32 antibodies (1:2000, ab223200, Abcam), cells were labeled with FITC anti-CD4 antibodies (1:100, ab59474, Abcam). After fixation and permeabilization, intracellular staining was performed with PE anti-IL-17 A antibodies. Similarly, Treg cells were labeled using surface markers FITC anti-CD4 and APC anti-CD25 antibodies (1:300, ab210330, Abcam) and nuclear marker PE anti-Foxp3 antibodies (1:500, ab218773, Abcam). Data were analyzed using FlowJo v10 software.

RNA Immunoprecipitation (RIP) detection of CTCF binding to circHECTD1 or METTL3 binding to claudin1 mRNA

When the cell confluence reached 80%–90%, the medium was discarded and the cells were rinsed with 1 mL of cold PBS and lysed with RIPA buffer in an ice bath for 5 min. The lysate was centrifuged at 32876.4 × *g* for 10 min at 4 °C. A portion of the cell extract was used as input, while another portion was incubated with CTCF (1:1000, ab128873, Abcam) or METTL3 (1:1000, ab195352, Abcam) antibodies. Proteinase K was used to extract RNA for PCR detection of circHECTD1 or claudin1 mRNA.

Chromatin Immunoprecipitation (ChIP) detection of CTCF binding to the METTL3 promoter

Experiments were performed according to the instructions of a ChIP kit (26156, Thermo Fisher Scientific). Cells (5×10^8) were cultured until adherent, and 1% paraformaldehyde was added to the medium. The cells were incubated at room temperature for 10 min, and glycine was added to terminate the crosslinking reaction. Chromatin fragments (300–1000 bp) were obtained by ultrasonication. IgG or CTCF antibodies (1:1000, ab128873, Abcam) were used for immunoprecipitation. Streptavidin beads were used to capture the immune complexes. After extensive washing, the bead complexes

were treated with 50 µL of DNA elution buffer at 37 °C for 30 min, boiled with 10 µL of 5X loading buffer at 100 °C for 10 min, and centrifuged. The supernatant was collected for RT-qPCR.

Luciferase reporter assay

The METTL3 promoter reporter plasmid and CTCF overexpression plasmid were purchased from RiboBio. The METTL3 promoter reporter plasmid was cloned into the pGL3 Basic vector. Forty-eight hours after co-transfection of the plasmids into MODE-K cells, the Renilla luciferase activity was detected using the Dual-Glo Luciferase Reporter Assay System (Promega), normalized to the internal control firefly luciferase activity.

Me-RIP detection of claudin1 m^{6}A modification

According to the instructions of the Magna MeRIP m^{6}A Kit (Millipore), bead-antibody complexes were prepared by incubating Magna ChIP protein A/G magnetic beads with anti-m^{6}A or normal IgG. Then, extracted cellular RNA was incubated with the bead-antibody complexes at 4 °C overnight, and total RNA was used as input. Eluted RNA was collected for the detection of m^{6}A in claudin1 mRNA.

RT-qPCR

Total RNA was extracted using TRIzol reagent (Invitrogen) and cDNA was synthesized using a PrimeScript RT reagent kit (Takara, Dalian, China). PCR was performed using SYBR Green (Takara) with specific primers (Table 3). Relative expression was calculated using the $2^{-\Delta\Delta Ct}$ method and normalized to β-actin.

Western blotting

Total protein was extracted with RIPA lysis buffer (Beyotime). After SDS-PAGE separation, proteins were transferred onto PVDF membranes. After skim milk blocking, the membranes were probed with primary antibodies (Abcam) including CD63 (1:5000, ab134045), TSG101 (1:1000, ab125011), HSP70 (1:500, ab2787), ZO-1 (1:1000, ab276131), occludin (1:1000, ab216327), claudin1 (1:1000, ab203563), METTL3 (1:1000, ab195352), CTCF (1:1000, ab300639), and β-actin (1:50000, ab8227), followed by the treatment with secondary antibodies (1:3000, ab205718). Protein bands were obtained using ECL reagent (Beyotime). Signal intensity was analyzed using Image J software.

Statistical analysis

Statistical analysis was performed using SPSS software version 25. Values are expressed as mean ± standard deviation. One-way analysis of variance and Tukey's post hoc test were employed to analyze statistical differences. P values of <0.05 were considered statistically significant.

Results

Identification of BMSCs and exosomes

First, the collected BMSCs were identified. The cells were observed to be spindle-shaped under a light microscope (Fig. 1A). Directional differentiation was induced to evaluate the multipotency of BMSCs. The isolated BMSCs were positive for Alizarin Red staining after osteogenic differentiation induction and Oil Red O staining after adipogenic differentiation induction (Fig. 1B-C), indicating that they have osteogenic and adipogenic differentiation capabilities. The expression of stem cell surface markers was further detected by flow cytometry. The positive rates of CD105, CD90, and CD29 reached more than 98%, and a few cells expressed CD45 (hematopoietic cell surface marker) or CD31 (endothelial cell surface marker) (Fig. 1D). Next, BMSC-derived exosomes were isolated. The morphology of the exosomes was observed by transmission electron microscopy and their

Table 3 Primer sequences used in the study

Primer	Sequence (5′–3′)
CircHECTD1-F	ACCAGCCTCACATCAACTTCCA
CircHECTD1-R	GTGGATCAAGAGGCCAAGTTGC
METTL3-F	TGGTGGTCCTAAGAGTTGAACC
METTL3-R	GGGGCATGAGACTGAAGCAG
CTCF-F	CAGCCACGGAGAGGTAAGTG
CTCF-R	GCAGGGATTACACCATGCCT
Claudin1-F	AAACCATGCCTGGAGCAGTC
Claudin1-R	GCATCCTCCTAGCAACCGTC
β-actin-F	GAAGGCTATAGTCACCTCGGG
β-actin-R	ATGGTAATAATGCGGCCGGT

F, forward primer; R, reverse primer

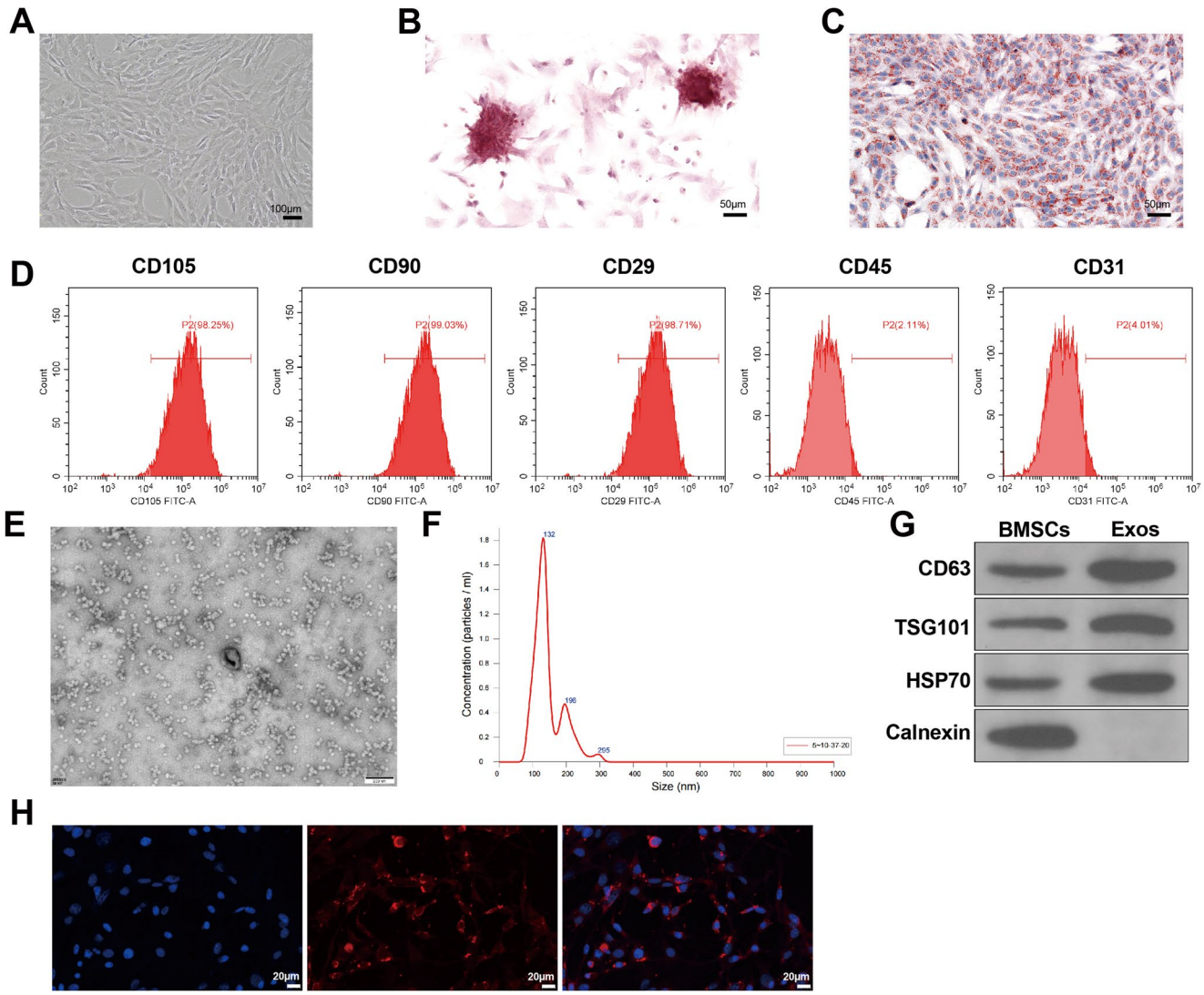

Fig. 1 Identification of BMSCs and exosomes. The obtained BMSCs and exosomes were identified: (A) BMSC morphology was observed by light microscopy. (B) Alizarin Red staining was performed after osteogenic differentiation. (C) Oil Red O staining was performed after adipogenic differentiation. (D) MSC markers were detected by flow cytometry. (E) Exosome morphology was observed by transmission electron microscopy. (F) Particle size analysis was performed to measure exosome sizes. (G) Exosome markers were detected by western blotting. (H) Immunofluorescence staining was used to visualize exosome (100 μg/mL) uptake by MODE-K cells

sizes were analyzed. The exosomes had a disc-like shape with a diameter of 50–200 nm (Fig. 1E-F). Western blotting results showed that the exosomes were positive for CD63, TSG101, and HSP70 and negative for calnexin (Fig. 1G). After incubation of MODE-K cells with PKH26-stained exosomes, it was shown that exosomes could be ingested by MODE-K cells (Fig. 1H).

Exo-circHECTD1 alleviates UC

Our previous study has shown that circHECTD1 is expressed at low levels in UC [15]. To explore the effect of circHECTD1 encapsulated in BMSC-derived exosomes on UC, the circHECTD1 overexpression vector was first transfected into BMSCs to obtain exosomes overexpressing circHECTD1 (Exo-circHECTD1) (Fig. 2A, $P < 0.05$). MODE-K cells were incubated with Exo-circHECTD1 and then stimulated with LPS to establish a cell model. Compared with the LPS group, the LPS + Exo group showed increases in viability and tight junction protein (ZO-1, occludin) expression and decreases in apoptosis, inflammatory factor (IL-1β, TNF-α) levels, and FD4 permeability (Fig. 2B-F, $P < 0.05$). Co-incubation with Exo-circHECTD1 further alleviated LPS-induced barrier damage among MODE-K cells.

Next, we established a colitis mouse model to study the effect of Exo-circHECTD1 on UC progression in vivo. Exosome treatment alleviated DSS-induced colitis, as shown by

increased colon length and body weight, decreased DAI, decreased IL-1β and TNF-α levels, increased ZO-1 and occludin expression, and decreased FD4 flux (Fig. 2G-L, $P<0.05$). Exo-circHECTD1 treatment further augmented the variations in these colitis-related indicators. Histological analysis showed that Exo-circHECTD1 was also superior in reducing colon mucosal damage and inflammatory cell infiltration (Fig. 2M, $P<0.05$). Taken together, these results indicate that Exo-circHECTD1 alleviates DSS-induced experimental colitis.

Claudin1 promotes the recovery of LPS-injured MODE-K cells

We previously detected low claudin1 expression in UC [17] but did not analyze its function in this disease. In this study, we first transfected claudin1-related vectors into MODE-K cells. RT-qPCR and western blotting showed that claudin1 expression increased following OE-claudin1 transfection and declined following sh-claudin1 transfection (Fig. 3A-B, $P < 0.05$). Transfected cells were then treated with LPS. Compared with the LPS group, the LPS + OE-claudin1 group showed increases in viability and ZO-1/occludin expression and decreases in apoptosis, IL-1β/TNF-α levels, and FD4 flux (Fig. 3C-G, $P < 0.05$). On the contrary, sh-claudin1 aggravated the damage to MODE-K cells (Fig. 3C-G, $P < 0.05$). This indicates that claudin1 can alleviate LPS-induced barrier damage among MODE-K cells.

CircHECTD1 modulates claudin1 expression via the CTCF/METTL3 axis

We detected an increase in claudin1 expression in MODE-K cells treated with Exo-circHECTD1 (Fig. 4A-B, $P < 0.05$). In mice, treatment with Exo-circHECTD1 alleviated DSS-induced suppression of claudin1 expression (Fig. 4C-D, $P < 0.05$). These data suggest that circHECTD1 promotes claudin1 expression. However, the mechanism of circHECTD1 regulating claudin1 is unclear. Increasing evidence shows that m^6A methylation, as an important mode of post-transcriptional regulation, is an important molecular regulatory mechanism underlying UC. The SRAMP database (http://www.cuilab.cn/sramp) predicted multiple m^6A modification sites in claudin1. Me-RIP to detect m^6A modification showed that Exo-circHECTD1 treatment reduced the m^6A modification level of claudin1 in LPS-stimulated cells (Fig. 4E, $P<0.05$). This suggests that Exo-circHECTD1 regulates claudin1 m^6A modification to promote claudin1 expression. The m^6A methyltransferase METTL3 is involved in the progression of UC [18]. To detect the regulatory effect of METTL3 on claudin1, RIP was first used to verify the binding of METTL3 to claudin1 mRNA. Abundant claudin1 mRNA was detected in the METTL3 antibody pull-down product (Fig. 4F, $P < 0.05$). METTL3-related vectors were then transfected into MODE-K cells. The m^6A modification level of claudin1 was elevated by OE-METTL3 transfection and reduced by sh-METTL3 transfection (Fig. 4G, $P < 0.05$). Moreover, METTL3 inhibited the expression of claudin1 (Fig. 4H-I, $P < 0.05$).

The starBase database (https://rnasysu.com/) predicted circHECTD1-binding sites in the transcription factor CTCF. RIP results showed that circHECTD1 was enriched in the CTCF antibody pull-down product (Fig. 4J, $P<0.05$), demonstrating that circHECTD1 directly binds to CTCF. The JASPAR database (https://jaspar.genereg.net/) showed that CTCF had binding sites in the METTL3 promoter. ChIP experiments verified the binding of CTCF to the METTL3 promoter (Fig. 4K, $P<0.05$). Luciferase reporter assay showed that CTCF promoted the activity of the METTL3 promoter (Fig. 4L, $P<0.05$). CTCF-related vectors were transfected into MODE-K cells. OE-CTCF transfection increased METTL3 expression and decreased claudin1 expression, whereas sh-CTCF group transfection reduced METTL3 expression and promoted claudin1 expression (Fig. 4M-N, $P<0.05$). Moreover, LPS stimulation increased the expression of CTCF and METTL3 in MODE-K cells; the expression of CTCF and METTL3 was decreased by Exo-circHECTD1 treatment in LPS-induced cells (Fig. 4O-P, $P<0.05$).

Collectively, these results demonstrate that circHECTD1 binds to CTCF to inhibit METTL3 transcription, thereby reducing claudin1 m^6A modification and promoting claudin1 expression.

CTCF or METTL3 knockdown promotes the recovery of LPS-injured MODE-K cells

To analyze the influences of CTCF and METTL3 on MODE-K cell barrier damage, we transfected MODE-K cells with sh-CTCF or sh-METTL3. Cell phenotype detection showed that CTCF or METTL3 knockdown enhanced viability, reduced apoptosis, decreased IL-1β and TNF-α levels, increased ZO-1 and occludin expression, and inhibited FD4 flux in MODE-K cells (Fig. 5A-E, $P<0.05$), indicating that knocking down CTCF or METTL3 can alleviate LPS-induced MODE-K cell barrier damage.

Exo-circHECTD1 targets claudin1 to alleviate UC

To determine whether Exo-circHECTD1 protects MODE-K cells by promoting claudin1 expression, MODE-K cells were transfected with sh-claudin1, incubated with

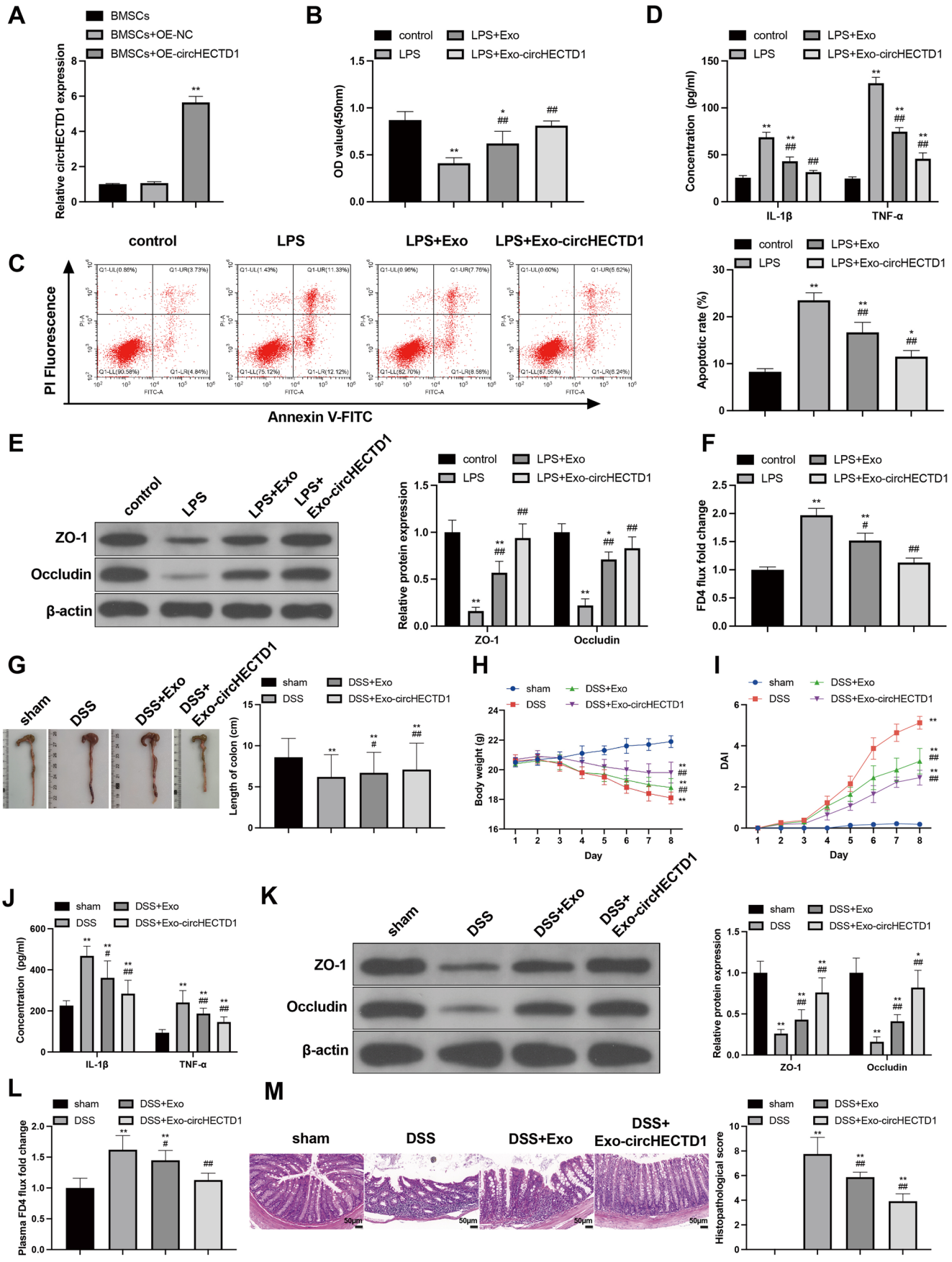
A
BMSCs
BMSCs+OE-NC
BMSCs+OE-circHECTD1
Relative circHECTD1 expression
B
control
LPS
LPS+Exo
LPS+Exo-circHECTD1
OD value(450nm)
C
control
LPS
LPS+Exo
LPS+Exo-circHECTD1
PI Fluorescence
Annexin V-FITC
D
Concentration (pg/ml)
IL-1β
TNF-α
Apoptotic rate (%)
E
ZO-1
Occludin
β-actin
Relative protein expression
F
FD4 flux fold change
G
sham
DSS
DSS+Exo
DSS+ Exo-circHECTD1
Length of colon (cm)
H
Body weight (g)
Day
I
DAI
J
Concentration (pg/ml)
K
Relative protein expression
L
Plasma FD4 flux fold change
M
Histopathological score
50μm

Fig. 2 Exo-circHECTD1 alleviates UC. In vitro experiments: MODE-K cells were treated with LPS (1 μg/mL) for 24 h as a cellular model and then incubated with exosomes (100 μg/mL) for 24 h for subsequent analysis. (A) Exosomal circHECTD1 expression was detected by RT-qPCR. (B) CCK-8 was used to assess cell viability after 48 h. (C) Apoptosis was analyzed by flow cytometry. (D) ELISA was performed to detect IL-1β and TNF-α (pg/mL). (E) ZO-1 and occludin were detected by western blotting. (F) FITC fluorescence intensity was measured to evaluate cell permeability. $N=3$. * $P<0.05$, ** $P<0.01$. In vivo experiments: Mice with UC were treated with Exo-circHECTD1 (from the day before the modeling began, 50 μg of exosomes were administered by gavage, once every two days. The detection was conducted on the 8th day of the modeling process.) (G) Colon length. (H) Body weight. (I) Disease activity index. (J) ELISA was performed to detect serum IL-1β and TNF-α (pg/mL). (K) ZO-1 and occludin were detected by western blotting. (L) FITC fluorescence intensity was measured to evaluate intestinal permeability. (M) H&E staining was conducted to visualize tissue damage. $N=8$. * $P<0.05$, ** $P<0.01$

Exo-circHECTD1, and then treated with LPS. Compared with the LPS + Exo-circHECTD1 group, the LPS + Exo-circHECTD1 + sh-claudin1 group showed reductions in viability and ZO-1/occludin expression and increases in apoptosis, IL-1β/TNF-α levels, and FD4 flux (Fig. 6A-E, $P<0.05$). This indicates that knocking down claudin1 can reverse the protective effect of Exo-circHECTD1 on LPS-treated MODE-K cells.

Claudin1 expression was inhibited by AAV infection to analyze the regulation of Exo-circHECTD1 on claudin1 in colitic mice. In comparison with the DSS + Exo-circHECTD1 group, the DSS + Exo-circHECTD1 + AAV-sh-claudin1 group showed reduced colon length and body weight, increased DAI, elevated IL-1β and TNF-α levels, reduced ZO-1 and occludin expression, increased FD4 flux, aggravated tissue damage, and increased inflammatory cell infiltration (Fig. 6F-L, $P<0.05$), indicating that claudin1 can reverse the alleviating effect of Exo-circHECTD1 on UC in vivo.

Exo-circHECTD1 targets claudin1 to regulate gut microbiota in mice with UC

The impact of Exo-circHECTD1 on gut microbiota was investigated. The composition of the gut microbiome at the phylum level is displayed in Fig. 7A. DSS treatment changed the relative abundance of Bacteroidetes, Firmicutes, Proteobacteria, Tenericutes, Deferribacteres, Candidatus Melainabacteria, and Actinobacteria (Fig. 7B-C, E-I, $P<0.05$) and increased the ratio of Firmicutes to Bacteroidetes (Fig. 7D, E-I, $P<0.05$). Compared with the

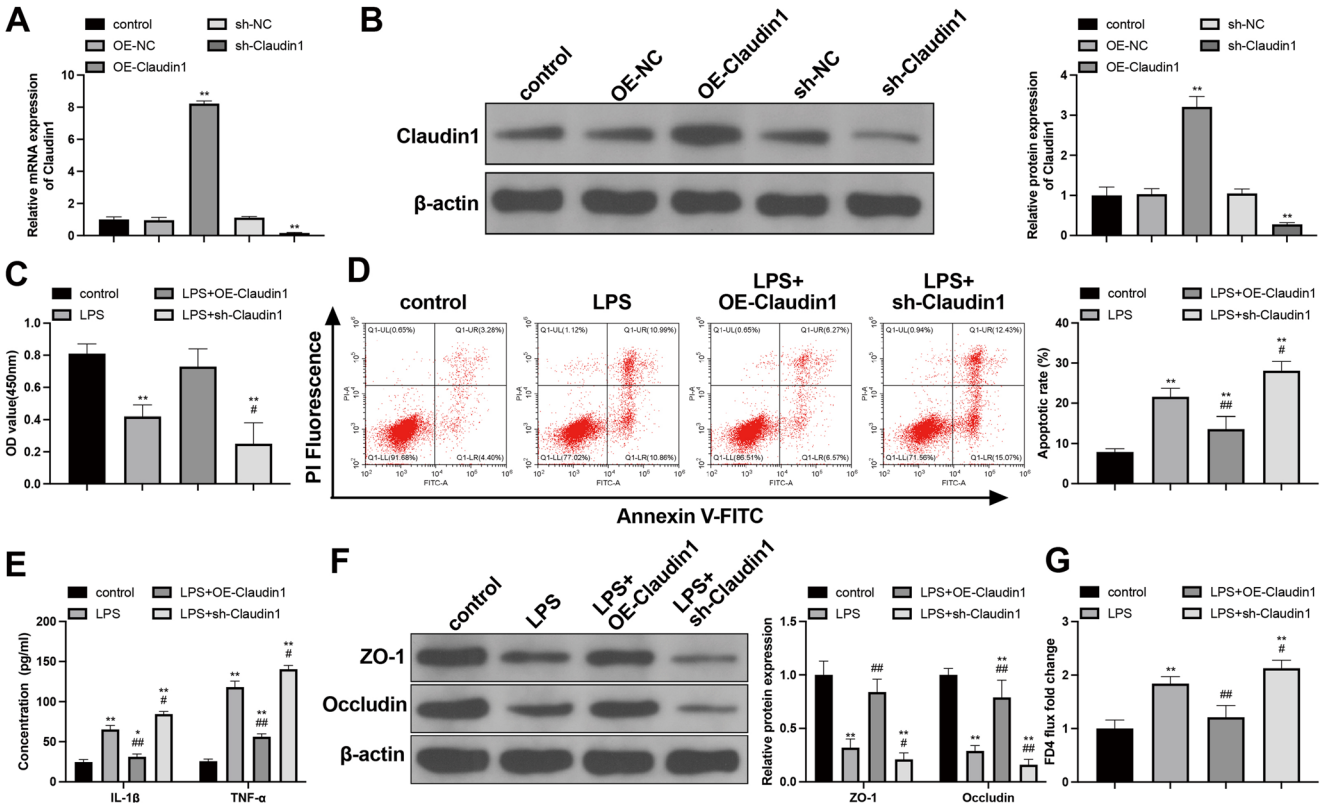

Fig. 3 Claudin1 alleviates LPS-induced MODE-K cell damage. MODE-K cells were transfected with claudin1-related vectors: (A-B) RT-qPCR (A) and western blotting (B) were employed to detect claudin1 mRNA and protein. (C) CCK-8 was used to assess cell viability after 48 h. (D) Apoptosis was analyzed by flow cytometry. (E) ELISA was performed to detect IL-1β and TNF-α (pg/mL). (F) ZO-1 and occludin were detected by western blotting. (G) FITC fluorescence intensity was measured using a fluorescence microplate reader. $N=3$. * $P<0.05$, ** $P<0.01$

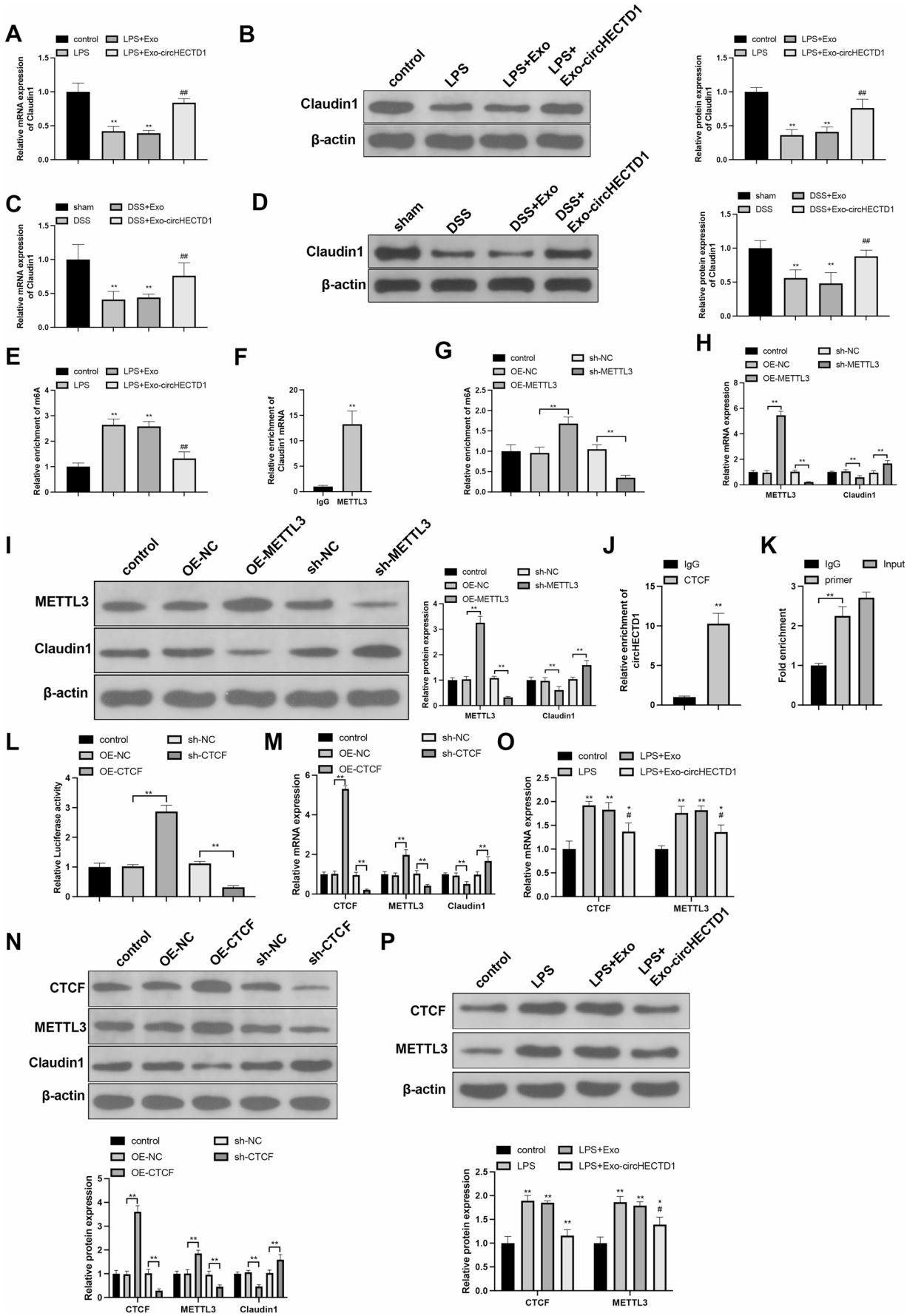
A
control
LPS
LPS+Exo
LPS+Exo-circHECTD1
Relative mRNA expression of Claudin1
B
control
LPS
LPS+Exo
LPS+ Exo-circHECTD1
Claudin1
β-actin
Relative protein expression of Claudin1
C
sham
DSS
DSS+Exo
DSS+Exo-circHECTD1
Relative mRNA expression of Claudin1
D
sham
DSS
DSS+Exo
DSS+ Exo-circHECTD1
Claudin1
β-actin
Relative protein expression of Claudin1
E
Relative enrichment of m6A
F
Relative enrichment of Claudin1 mRNA
IgG
METTL3
G
sh-NC
OE-NC
sh-METTL3
OE-METTL3
Relative enrichment of m6A
H
Relative mRNA expression
METTL3
Claudin1
I
control
OE-NC
OE-METTL3
sh-NC
sh-METTL3
METTL3
Claudin1
β-actin
Relative protein expression
J
IgG
CTCF
Relative enrichment of circHECTD1
K
IgG
Input
primer
Fold enrichment
L
sh-CTCF
OE-CTCF
Relative Luciferase activity
M
Relative mRNA expression
CTCF
METTL3
Claudin1
O
Relative mRNA expression
N
CTCF
METTL3
Claudin1
β-actin
Relative protein expression
P
CTCF
METTL3
β-actin
Relative protein expression

Fig. 4 CircHECTD1 regulates claudin1 through CTCF/METTL3. The mechanism of circHECTD1 regulating claudin1: (A-D, H-I, M-P) RT-qPCR (A, C, H, M, O) and western blotting (B, D, I, N, P) were used to measure mRNA and protein expression. (E, G) Me-RIP was used to detect claudin1 m^{6}A modification. (F) RIP was used to detect the binding of METTL3 to claudin1 mRNA. (J) RIP was used to detect the binding of circHECTD1 to CTCF. (K) ChIP was used to verify the binding of CTCF to the METTL3 promoter. (L) METTL3 promoter activity was analyzed using luciferase reporters. $N=3$. * $P<0.05$, ** $P<0.01$

DSS group, the DSS + Exo-circHECTD1 group showed an increase in the relative abundance of Bacteroidetes and decreases in the relative abundance of Proteobacteria and Candidatus Melainabacteria and the ratio of Firmicutes to Bacteroidetes (Fig. 7B-I, $P<0.05$). Infection with AAV-sh-claudin1 reversed the regulatory effect of Exo-circHECTD1 on the gut microbiome. This indicates that Exo-circHECTD1 targets claudin1 to regulate the gut microbiota of colitic mice.

Exo-circHECTD1 targets claudin1 to modulate the balance of Th17/Treg cells in mice with UC

Imbalance between Th17 and Treg cell differentiation, imbalance of gut microbiota, and damage to the intestinal mucosal barrier may be important contributors to the development of inflammatory bowel disease. Moreover, Th17 and Treg differentiation are affected by gut microbiota. The ratio of Th17/Treg cells in lymphocytes was measured to determine whether Exo-circHECTD1 regulates Th17/Treg balance in colitic mice. DSS treatment increased Th17 cells and reduced Treg cells. The DSS + Exo-circHECTD1 group had a decreased ratio of Th17/Treg cells relative to the DSS group. In comparison with the DSS + Exo-circHECTD1 group, the DSS + Exo-circHECTD1 + AAV-sh-claudin1 group showed an increase in the Th17/Treg cell ratio (Fig. 8A-J, $P<0.05$). This indicates that Exo-circHECTD1 targets claudin1 to regulate Th17/Treg balance in colitic mice.

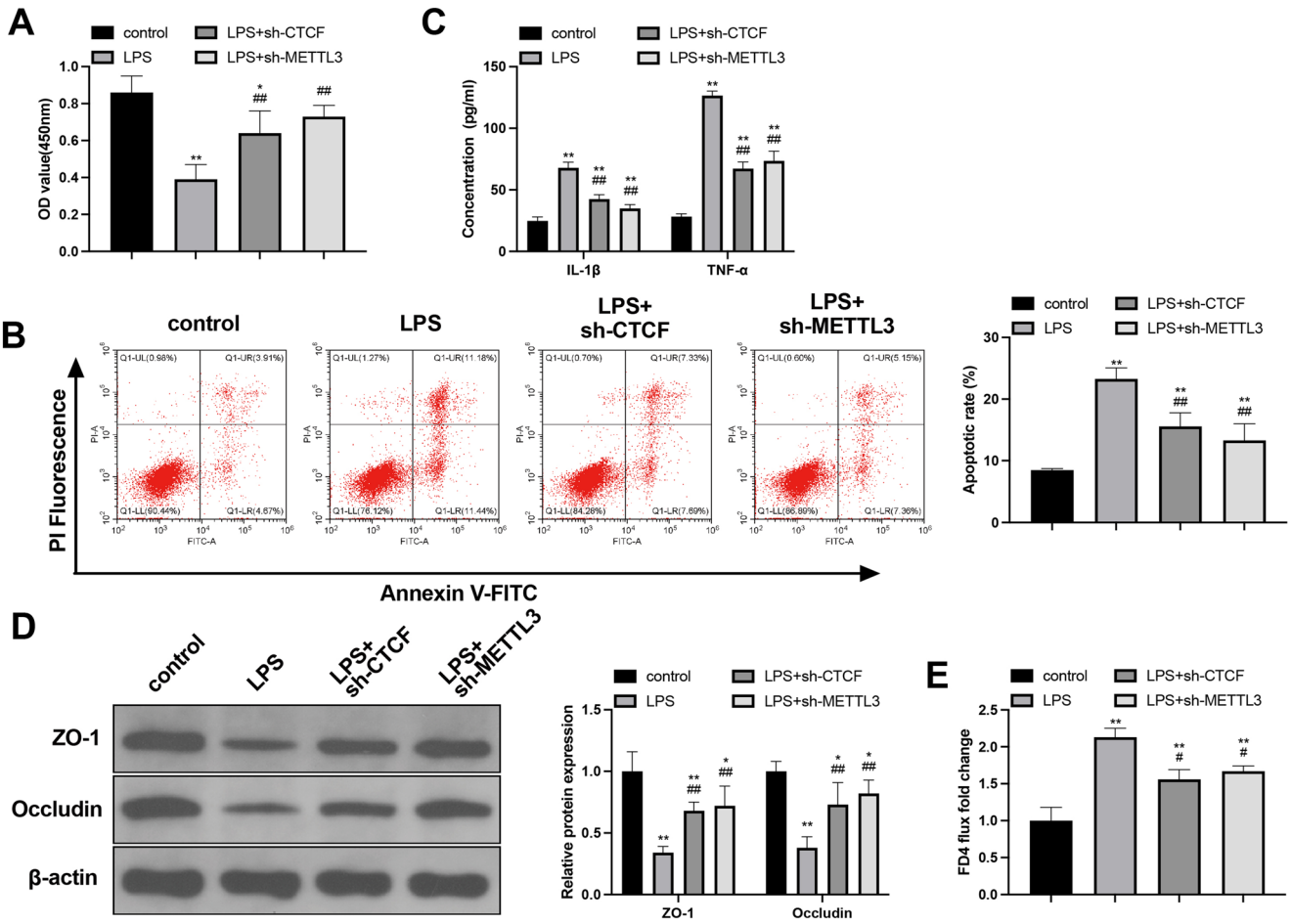

Fig. 5 CTCF or METTL3 knockdown alleviates LPS-induced MODE-K cell damage. sh-CTCF or sh-METTL3 was introduced into MODE-K cells: (A) CCK-8 was used to assess cell viability after 48 h. (B) Apoptosis was analyzed by flow cytometry. (C) ELISA was performed to detect IL-1β and TNF-α (pg/mL). (D) ZO-1 and occludin were detected by western blotting. (E) FITC fluorescence intensity was measured using a fluorescence microplate reader. $N=3$. * $P<0.05$, ** $P<0.01$

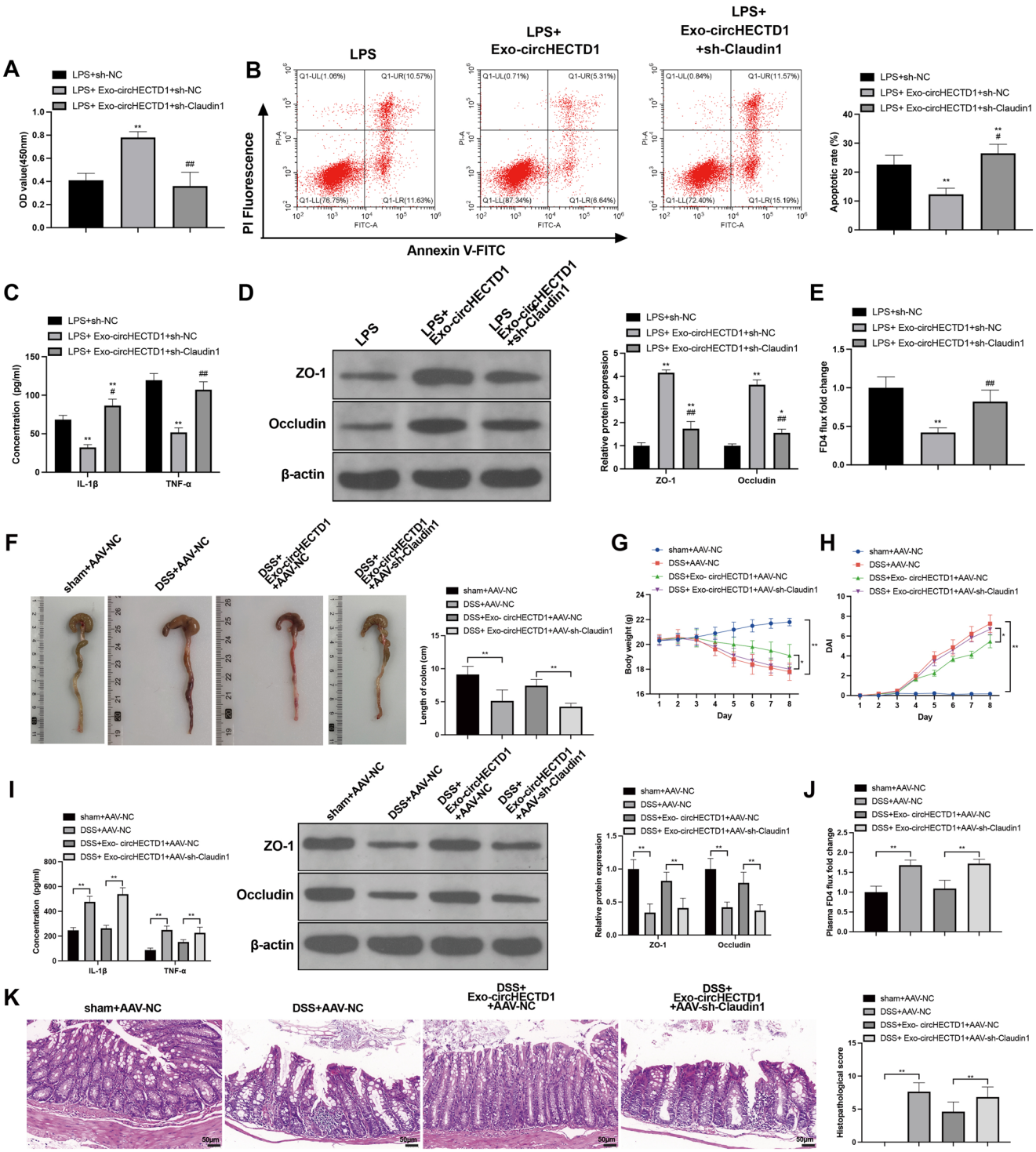

Fig. 6 Exo-circHECTD1 targets claudin1 to slow down UC progression. MODE-K cells were transfected with sh-claudin1 and then incubated with Exo-circHECTD1: (A) CCK-8 was used to assess cell viability after 48 h. (B) Apoptosis was analyzed by flow cytometry. (C) ELISA was performed to detect IL-1β and TNF-α (pg/mL). (D) ZO-1 and occludin were detected by western blotting. (E) FITC fluorescence intensity was measured using a fluorescence microplate reader. $N=3$. * $P<0.05$, ** $P<0.01$. After claudin1 knockdown by AAVs, mice with UC were treated with Exo-circHECTD1: (F) Colon length (cm). (G) Body weight (g). (H) Disease activity index. (I) ELISA was performed to detect IL-1β and TNF-α (pg/mL). (J) ZO-1 and occludin were detected by western blotting. (K) FITC fluorescence intensity was measured. (L) Tissue damage was analyzed by H&E staining. $N=8$. * $P<0.05$, ** $P<0.01$

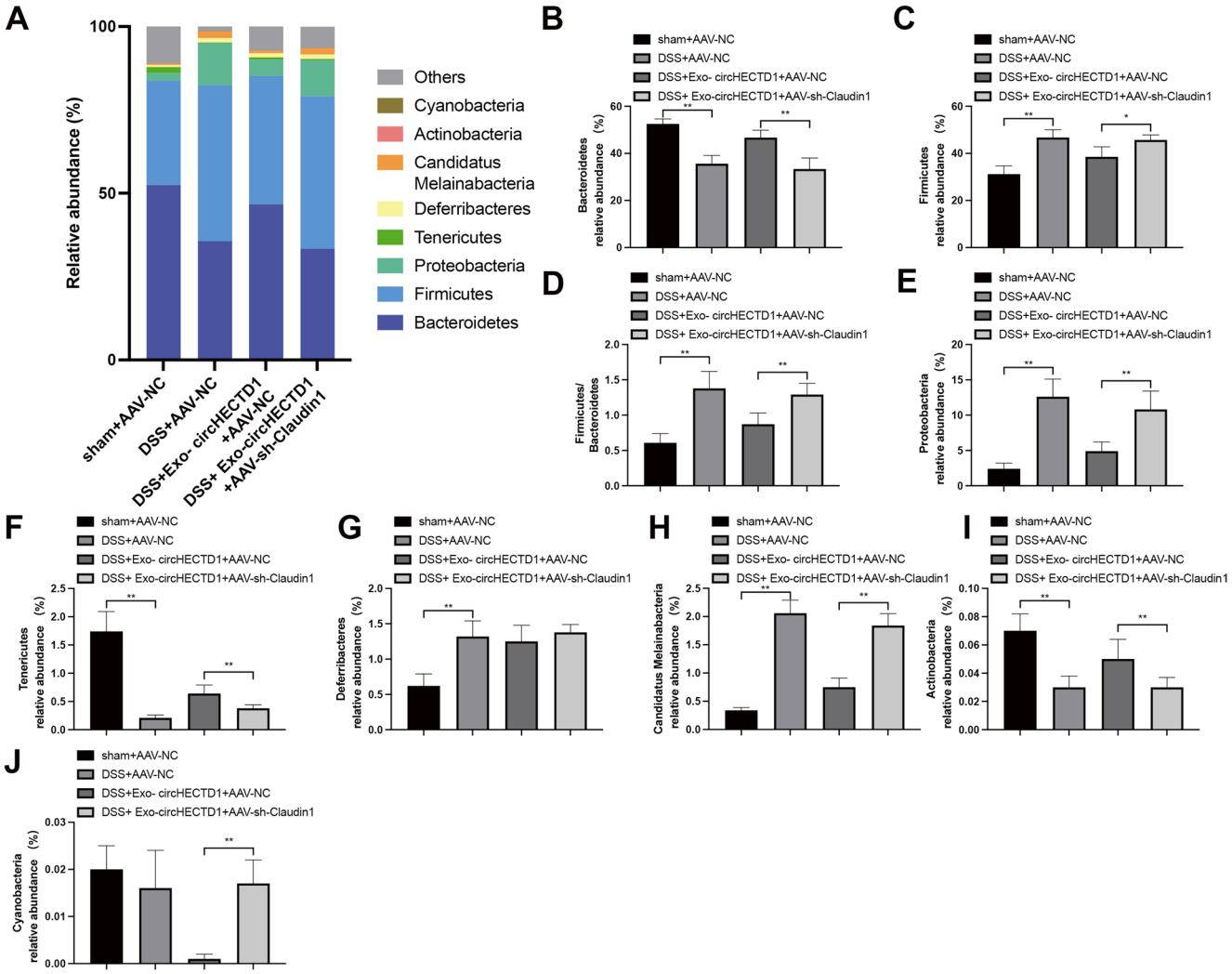

Fig. 7 Exo-circHECTD1 targets claudin1 to regulate the microbial composition of mice with UC. Relative abundance of gut microbiota in the feces of mice from each group: (A) Relative abundance of fecal microbiota at the phylum level. Relative abundance of Bacteroidetes (B) and Firmicutes (C). (D) Ratio of Firmicutes to Bacteroidetes at the phylum level. Relative abundance of Proteobacteria (E), Tenericutes (F), Deferribacteres (G), Candidatus Melainabacia (H), Actinobacteria (I), and Cyanobacteria (J). $N=8$. * $P<0.05$, ** $P<0.01$

Discussion

UC is a chronic, relapsing gastrointestinal inflammatory disease, for which there is currently no cure and no gold standard diagnostic test [19]. Therefore, there is an urgent need for effective diagnostic tools and treatments. MSC-derived exosomes have recently emerged as a promising therapeutic tool. In this study, we isolated BMSC-derived exosomes to analyze their effect on UC in vivo and in vitro. The therapeutic effect of BMSC-derived exosomes on UC was partially due to circHECTD1, which can bind to the transcription factor CTCF to inhibit METTL3 transcription and subsequently reduce m^6A modification to promote the expression of the tight junction protein claudin1.

This study first demonstrated the therapeutic effect of BMSC-derived exosomes on UC. Exosome treatment alleviated LPS-induced barrier damage among intestinal epithelial MODE-K cells and reduced colonic mucosal damage and inflammatory cell infiltration in mice with DSS-induced UC. Moreover, exosome treatment restored the balance of gut microbiota and Th17/Treg cells in mice with UC. Previous studies have also revealed that MSC-derived exosomes can alleviate UC by regulating Treg cells, inflammation, and epithelial regeneration [12, 20, 21]. The efficacy of exosomes is largely dependent on their cargos, such as proteins, RNA, and DNA [22]. BMSC-derived exosomes can deliver EphB2 or miR-181a to enhance intestinal barrier function and regulate immune balance in UC models [23, 24]. Hypoxia-preconditioned MSCs can release exosomes containing miR-214-3p or HIF-1α to reduce oxidative stress damage and alleviate UC [25, 26]. By far, the mechanisms of action of MSC-derived exosomes in UC remain poorly

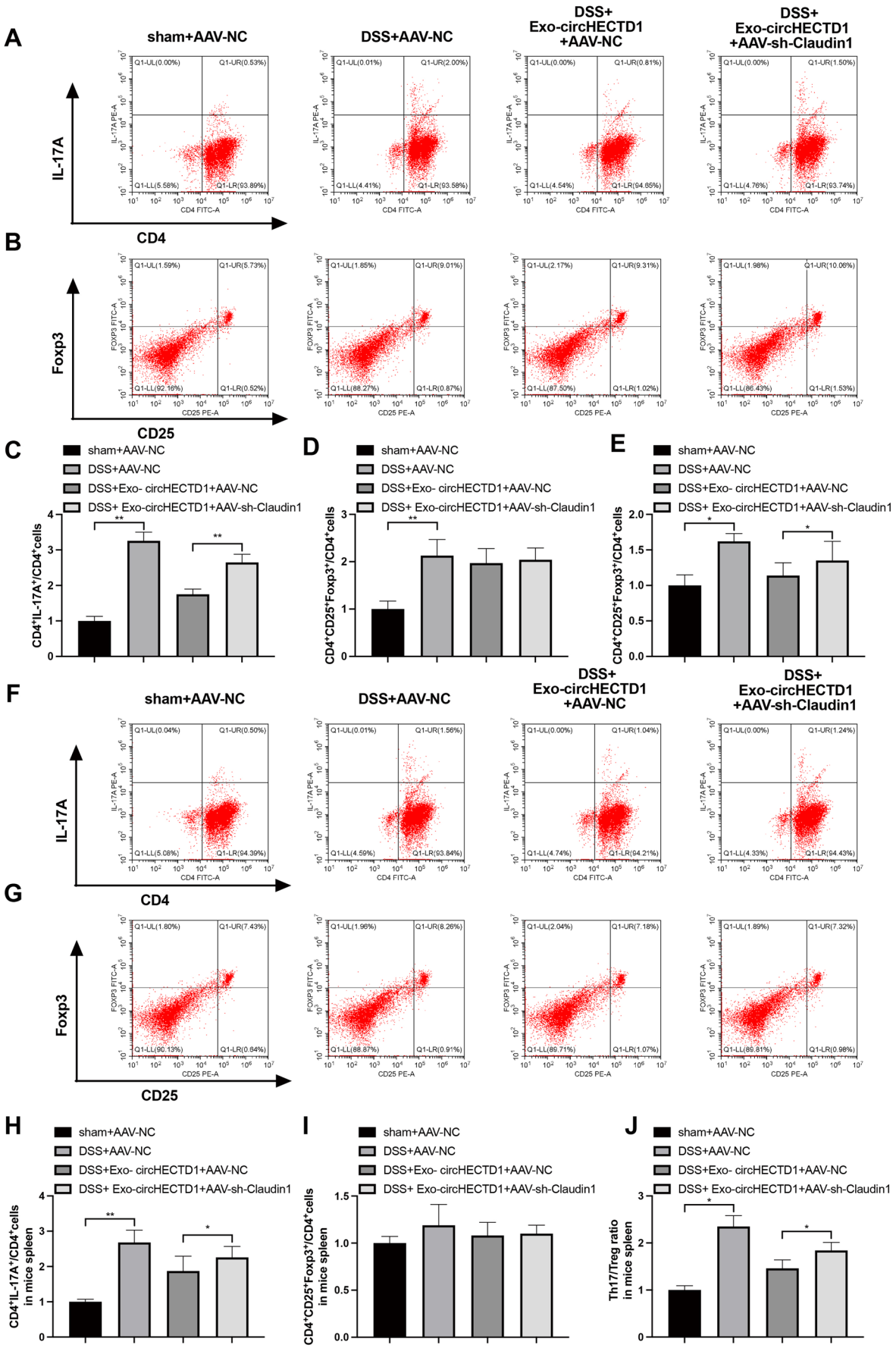
A
sham+AAV-NC
DSS+AAV-NC
DSS+ Exo-circHECTD1 +AAV-NC
DSS+ Exo-circHECTD1 +AAV-sh-Claudin1
IL-17A
CD4
B
Foxp3
CD25
C
sham+AAV-NC
DSS+AAV-NC
DSS+Exo- circHECTD1+AAV-NC
DSS+ Exo-circHECTD1+AAV-sh-Claudin1
CD4+IL-17A+/CD4+cells
D
CD4+CD25+Foxp3+/CD4+cells
E
CD4+CD25+Foxp3+/CD4+cells
F
G
H
CD4+IL-17A+/CD4+cells in mice spleen
I
CD4+CD25+Foxp3+/CD4+cells in mice spleen
J
Th17/Treg ratio in mice spleen

Fig. 8 Exo-circHECTD1 targets claudin1 to regulate the differentiation of Th17 and Treg cells. (A-B) Flow cytometry was used to measure the proportions of Th17 and Treg cells in mesenteric lymph nodes. (C-D) Statistical analysis of Th17 (C) and Treg (D) cell proportions in mesenteric lymph nodes. (E) The ratio of Th17/Treg cells in mesenteric lymph nodes. (F-G) Flow cytometry was used to measure the proportions of Th17 and Treg cells in colonic lamina propria lymphocytes. (H-I) Statistical analysis of Th17 (H) and Treg (I) cell proportions in colonic lamina propria lymphocytes. (J) The ratio of Th17/Treg cells in colonic lamina propria lymphocytes. $N=8$. * $P<0.05$, ** $P<0.01$

studied and warrant further investigations to promote their application in clinical settings.

This study identified circHECTD1 as responsible for the therapeutic effect of BMSC-derived exosomes on UC. Exosomes from BMSCs overexpressing circHECTD1 were more effective than untreated exosomes against UC both in vivo and in vitro. CircHECTD1 has exhibited multiple functions. It acts as an oncogene in several cancers including gastric cancer [27, 28], glioma [29], hepatocellular carcinoma [30], and glioblastoma multiforme [31]. In response to SiO_2 exposure, circHECTD1 may be downregulated to promote pulmonary fibroblast activation and subsequent fibrosis [32]. Knockdown of circHECTD1 can be protective to neurons under ischemic conditions [33] and also improve cerebrovascular function against atherosclerosis and ischemic stroke [34]. Moreover, circHECTD1 is involved in immune and inflammatory responses [35–37], which is consistent with our findings that circHECTD1 plays an immune regulatory role in UC. Previously, we detected that circHECTD1 alleviated UC by promoting HuR expression through inhibition of miR-182-5p [15]. In this study, we found that exosomal circHECTD1 promoted claudin1 expression.

It is notable that claudin1 could mitigate LPS-induced barrier damage among MODE-K cells. Claudin1 knockdown nullified the therapeutic effect of Exo-circHECTD1 on UC both in vivo and in vitro. Moreover, claudin1 knockdown disrupted the balance of gut microbiota and Th17/Treg cells in mice with UC in the presence of Exo-circHECTD1. These findings suggest that Exo-circHECTD1 alleviates UC by promoting claudin1 expression. Claudin1 is a member of the claudin family, a group of membrane proteins involved in tight junction formation, and is predominantly expressed in endothelial or epithelial cells [38]. Tight junction remodeling in response to environmental changes is essential for maintaining the intestinal epithelial barrier against potentially harmful molecules in the lumen [8]. Barrier defects with corresponding claudin1 downregulation are frequently detected in UC [11, 39]. Our previous study also detected decreased claudin1 expression in UC and linked this to CIRP upregulation and HuR downregulation [17]. Therefore, the mechanism by which Exo-circHECTD1 regulates claudin1 was further investigated.

m^6A methylation is an important RNA modification that plays a potential role in UC [40]. A m^6A methyltransferase complex is comprised of a METTL3-METTL14 heterodimer core and other binding partners [41]. A previous study found that METTL3 increased the inflammatory response of LPS-stimulated MODE-K cells and promoted DSS-induced inflammatory bowel disease in mice [18]. Therefore, we wondered whether claudin1 can be regulated by m^6A. The SRAMP database predicted multiple m^6A modification sites in claudin1 mRNA. RIP assay verified that METTL3 can bind to claudin1 mRNA. METTL3 promoted the m^6A modification of claudin1 mRNA and inhibited claudin1 expression in LPS-stimulated MODE-K cells. Moreover, METTL3 downregulation alleviated LPS-induced MODE-K cell damage, which is consistent with the aforementioned findings about METTL3. METTL3 expression can be affected by H3K4me3-mediated transcription [42]. The transcription factor CTCF has been reported to modulate H3K27me3 modification in UC [43]. We found that CTCF can bind to the METTL3 promoter and promote METTL3 transcription. Moreover, CTCF knockdown alleviated LPS-induced MODE-K cell damage, which is consistent with the previous findings that CTCF is conducive to colonic mucosal epithelial injury in UC [43]. CircRNAs can serve as protein decoys, scaffolds, or recruiters, thereby regulating gene expression [44]. We found that circHECTD1 can bind to CTCF and inhibit CTCF expression.

In conclusion, BMSC-derived exosomal circHECTD1 inhibits METTL3 transcription by binding to CTCF to reduce claudin1 m^6A modification and promote claudin1 expression, thereby improving intestinal barrier function and alleviating UC. These findings suggest that exosomes can be used as a new medication for UC. This study also offers new insights into the pathogenesis of UC, which may help the development of new drugs targeting these molecular interactions.

Limitations

BMSC-exosomes can be engineered to deliver circHECTD1, thereby alleviating UC. The promise of BMSC-exosomal circHECTD1 as a UC therapy is supported by advantages such as the superior stability and low immunogenicity of circRNAs and the biocompatibility and safety of exosomes as natural biological nanoparticles. However, the low cargo capacity and potential off-target effects of exosomes may limit the use of exosomal circHECTD1 therapy. Additionally, the identification of Th17 cells in this study was preliminary, which could not exclude the presence of ILC3 population. Therefore, the observed effects of Th17 shall be carefully treated.

Supplementary Information The online version contains supplementary material available at https://doi.org/10.1007/s00018-025-06023-x.

Acknowledgements Not applicable.

Author contributions Ouyang, M., Li, F. and Xu, Y. conceived and designed the study. Wang, K., Liu, F., Deng, J., Peng, J., Wang, M. and Zhou, H. performed the experiments. Wang, K., Liu, F., Deng, J., Peng, J. and Wang, M. analyzed the data. Wang, K. and Liu, F. drafted the manuscript. Deng, J., Peng, J. and Zhou H. revised the manuscript. Ouyang, M., Li, F. and Xu, Y. supervised the study. All authors reviewed and approved the final version of the manuscript.

Funding This study was supported by grants from the National Natural Science Foundation of China (Nos. 81800471, 81974065, 82370566) and the Hunan Provincial Natural Science Foundation (No. 2022JJ30935, 2025JJ50700).

Data availability The datasets used or analyzed during the current study are available from the corresponding author on reasonable request.

Declarations

Ethics approval and consent to participate All animal experiments were authorized by the Ethics Committee of Xiangya Hospital, Central South University and were carried out in strict accordance with the Guidelines for the Ethical Review of Laboratory Animal Welfare in China.

Consent for publication Not applicable.

Conflict of interest The authors declare no conflict of interest.

References

1. Le Berre C, Honap S, Peyrin-Biroulet L (2023) Ulcerative colitis. Lancet 402:571–584
2. Du L, Ha C (2020) Epidemiology and pathogenesis of ulcerative colitis. Gastroenterol Clin North Am 49:643–654
3. Segal JP, LeBlanc JF, Hart AL (2021) Ulcerative colitis: an update. Clin Med (Lond) 21:135–139
4. Kucharzik T, Koletzko S, Kannengiesser K, Dignass A (2020) Ulcerative Colitis-Diagnostic and therapeutic algorithms. Dtsch Arztebl Int 117:564–574
5. Kobayashi T, Siegmund B, Le Berre C, Wei SC, Ferrante M, Shen B, Bernstein CN, Danese S, Peyrin-Biroulet L, Hibi T (2020) Ulcerative colitis. Nat Rev Dis Primers 6:74
6. van der Post S, Jabbar KS, Birchenough G, Arike L, Akhtar N, Sjovall H, Johansson MEV, Hansson GC (2019) Structural weakening of the colonic mucus barrier is an early event in ulcerative colitis pathogenesis. Gut 68:2142–2151
7. Nystrom EEL, Martinez-Abad B, Arike L, Birchenough GMH, Nonnecke EB, Castillo PA, Svensson F, Bevins CL, Hansson GC, Johansson MEV (2021) An intercrypt subpopulation of goblet cells is essential for colonic mucus barrier function. Science 372:eabb1590. https://doi.org/10.1126/science.abb1590
8. Allam-Ndoul B, Castonguay-Paradis S, Veilleux A (2020) Gut microbiota and intestinal trans-epithelial permeability. Int J Mol Sci 21:6402. https://doi.org/10.3390/ijms21176402
9. Nishii N, Oshima T, Li M, Eda H, Nakamura K, Tamura A, Ogawa T, Yamasaki T, Kondo T, Kono T, Tozawa K, Tomita T, Fukui H, Miwa H (2020) Lubiprostone induces Claudin-1 and protects intestinal barrier function. Pharmacology 105:102–108
10. Deng L, He S, Li Y, Ding R, Li X, Guo N, Luo L (2023) Identification of Lipocalin 2 as a potential Ferroptosis-related gene in ulcerative colitis. Inflamm Bowel Dis 29:1446–1457
11. Wang J, Zhang C, Guo C, Li X (2019) Chitosan ameliorates DSS-induced ulcerative colitis mice by enhancing intestinal barrier function and improving microflora. Int J Mol Sci 20:5751. https://doi.org/10.3390/ijms20225751
12. El-Desoky Mohamady RE, Elwia SK, Abo El Wafa SM, Mohamed MA (2022) Effect of mesenchymal stem cells derived exosomes and green tea polyphenols on acetic acid induced ulcerative colitis in adult male albino rats. Ultrastruct Pathol 46:147–163
13. Kalluri R, LeBleu VS (2020) The biology, function, and biomedical applications of exosomes. Science 367:eaau6977. https://doi.org/10.1126/science.aau6977
14. Niu D, Wu Y, Lian J (2023) Circular RNA vaccine in disease prevention and treatment. Signal Transduct Target Ther 8:341
15. Xu Y, Tian Y, Li F, Wang Y, Yang J, Gong H, Wan X, Ouyang M (2022) Circular RNA HECTD1 mitigates ulcerative colitis by promoting enterocyte autophagy via miR-182-5p/HuR axis. Inflamm Bowel Dis 28:273–288
16. Dieleman LA, Palmen MJ, Akol H, Bloemena E, Pena AS, Meuwissen SG, Van Rees EP (1998) Chronic experimental colitis induced by dextran sulphate sodium (DSS) is characterized by Th1 and Th2 cytokines. Clin Exp Immunol 114:385–91
17. Xu Y, Tian Y, Wang Y, Yang J, Li F, Wan X, Ouyang M (2021) Human antigen R (HuR) and cold inducible RNA-binding protein (CIRP) influence intestinal mucosal barrier function in ulcerative colitis by competitive regulation on Claudin1. BioFactors 47:427–443
18. Yang L, Wu G, Wu Q, Peng L, Yuan L (2022) METTL3 overexpression aggravates LPS-induced cellular inflammation in mouse intestinal epithelial cells and DSS-induced IBD in mice. Cell Death Discov 8:62
19. Wangchuk P, Yeshi K, Loukas A (2024) Ulcerative colitis: clinical biomarkers, therapeutic targets, and emerging treatments. Trends Pharmacol Sci 45:892–903
20. Heidari N, Abbasi-Kenarsari H, Namaki S, Baghaei K, Zali MR, Ghaffari Khaligh S, Hashemi SM (2021) Adipose-derived mesenchymal stem cell-secreted exosome alleviates dextran sulfate sodium-induced acute colitis by Treg cell induction and inflammatory cytokine reduction. J Cell Physiol 236:5906–5920
21. Barnhoorn MC, Plug L, Jonge E, Molenkamp D, Bos E, Schoonderwoerd MJA, Corver WE, van der Meulen-de Jong AE, Verspaget HW, Hawinkels L (2020) Mesenchymal stromal Cell-Derived exosomes contribute to epithelial regeneration in experimental inflammatory bowel disease. Cell Mol Gastroenterol Hepatol 9:715–717e8

22. Tan F, Li X, Wang Z, Li J, Shahzad K, Zheng J (2024) Clinical applications of stem cell-derived exosomes. Signal Transduct Target Ther 9:17
23. Chu S, Yu T, Wang W, Wu H, Zhu F, Wei C, Gao F, Liu C, Fan H (2023) Exosomes derived from EphB2-overexpressing bone marrow mesenchymal stem cells regulate immune balance and repair barrier function. Biotechnol Lett 45:601–617
24. Gu L, Ren F, Fang X, Yuan L, Liu G, Wang S (2021) Exosomal MicroRNA-181a derived from mesenchymal stem cells improves gut microbiota composition, barrier function, and inflammatory status in an experimental colitis model. Front Med (Lausanne) 8:660614
25. Li N, Zhao L, Geng X, Liu J, Zhang X, Hu Y, Qi J, Chen H, Qiu J, Zhang X, Jin S (2024) Stimulation by exosomes from hypoxia-preconditioned hair follicle mesenchymal stem cells facilitates mitophagy by inhibiting the PI3K/AKT/mTOR signaling pathway to alleviate ulcerative colitis. Theranostics 14:4278–4296
26. Zhu F, Wei C, Wu H, Shuai B, Yu T, Gao F, Yuan Y, Zuo D, Liu X, Zhang L, Fan H (2022) Hypoxic mesenchymal stem cell-derived exosomes alleviate ulcerative colitis injury by limiting intestinal epithelial cells reactive oxygen species accumulation and DNA damage through HIF-1alpha. Int Immunopharmacol 113:109426
27. Ruan X, Liu Y, Wang P, Liu L, Ma T, Xue Y, Dong W, Zhao Y, E T, Lin H, Wang D, Yang C, Song J, Liu J, Deng M, An P, Lin Y, Yang J, Cui Z, Cao Y, Liu X (2023) RBMS3-induced circHECTD1 encoded a novel protein to suppress the vasculogenic mimicry formation in glioblastoma multiforme. Cell Death Dis 14:745
28. Lu Y, Li L, Li L, Wu G, Liu G (2021) Circular RNA circHECTD1 prevents Diosbulbin-B-sensitivity via miR-137/PBX3 axis in gastric cancer. Cancer Cell Int 21:264
29. Li C, Liu Y, Lv Z, Zheng H, Li Z, Zhang J, Bao H, Zhang S, Xiong J, Jin H, Yu L, Ai S, Wang Y, Xiao X, Su T, Liang P (2021) Circular RNA circHECTD1 facilitates glioma progression by regulating the miR-296-3p/SLC10A7 axis. J Cell Physiol 236:5953–5965
30. Jiang QL, Feng SJ, Yang ZY, Xu Q, Wang SZ (2020) CircHECTD1 up-regulates mucin 1 expression to accelerate hepatocellular carcinoma development by targeting microRNA-485-5p via a competing endogenous RNA mechanism. Chin Med J (Engl) 133:1774–1785
31. Li W, Wang S, Shan B, Cheng X, He H, Qin J, Tang Y, Zhao H, Tian M, Zhang X, Jin G (2021) CircHECTD1 regulates cell proliferation and migration by the miR-320-5p/SLC2A1 axis in glioblastoma multiform. Front Oncol 11:666391
32. Chu H, Wang W, Luo W, Zhang W, Cheng Y, Huang J, Wang J, Dai X, Fang S, Chao J (2019) CircHECTD1 mediates pulmonary fibroblast activation via HECTD1. Ther Adv Chronic Dis 10:2040622319891558
33. Dai Q, Ma Y, Xu Z, Zhang L, Yang H, Liu Q, Wang J (2021) Downregulation of circular RNA HECTD1 induces neuroprotection against ischemic stroke through the microRNA-133b/TRAF3 pathway. Life Sci 264:118626
34. Feng M, Tu W, Zhou Q, Du Y, Xu K, Wang Y (2023) circHECTD1 promotes the proliferation and migration of human brain vascular smooth muscle cells via interacting with KHDRBS3 to stabilize EZH2 mRNA expression. J Inflamm Res 16:1311–1323
35. Lan S, Zhong G (2024) Identification of a novel survival and immune microenvironment related CeRNA regulatory network for hepatocellular carcinoma based on circHECTD1. Heliyon 10:e33763
36. Yang YN, Luo YB, Xu G, Li K, Ma RL, Yuan W (2023) CircHECTD1 promoted MIRI-associated inflammation via inhibiting miR-138-5p and upregulating ROCK2. Kaohsiung J Med Sci 39:675–687
37. Li H, Niu X, Shi H, Feng M, Du Y, Sun R, Ma N, Wang H, Wei D, Gao M (2022) CircHECTD1 attenuates apoptosis of alveolar epithelial cells in acute lung injury. Lab Invest 102:945–956
38. Bhat AA, Syed N, Therachiyil L, Nisar S, Hashem S, Macha MA, Yadav SK, Krishnankutty R, Muralitharan S, Al-Naemi H, Bagga P, Reddy R, Dhawan P, Akobeng A, Uddin S, Frenneaux MP, El-Rifai W, Haris M (2020) Claudin-1, a double-edged sword in cancer. Int J Mol Sci 21:569. https://doi.org/10.3390/ijms21020569
39. Xiong T, Zheng X, Zhang K, Wu H, Dong Y, Zhou F, Cheng B, Li L, Xu W, Su J, Huang J, Jiang Z, Li B, Zhang B, Lv G, Chen S (2022) Ganluyin ameliorates DSS-induced ulcerative colitis by inhibiting the enteric-origin LPS/TLR4/NF-kappaB pathway. J Ethnopharmacol 289:115001
40. Gu C, Wu J, Zhang W, Yao Y, Yan W, Yuan Y, Wang W, Shang A (2022) Immune infiltration of ulcerative colitis and detection of the m6A subtype. J Immunol Res 2022:7280977
41. Zeng C, Huang W, Li Y, Weng H (2020) Roles of METTL3 in cancer: mechanisms and therapeutic targeting. J Hematol Oncol 13:117
42. Xu QC, Tien YC, Shi YH, Chen S, Zhu YQ, Huang XT, Huang CS, Zhao W, Yin XY (2022) METTL3 promotes intrahepatic cholangiocarcinoma progression by regulating IFIT2 expression in an m(6)A-YTHDF2-dependent manner. Oncogene 41:1622–1633
43. Gu D, Cao T, Yi S, Liu Y, Fan C (2023) CCCTC-binding factor mediates the transcription of Insulin-Like growth factor binding protein 5 through EZH2 in ulcerative colitis. Dig Dis Sci 68:778–790
44. Zhou WY, Cai ZR, Liu J, Wang DS, Ju HQ, Xu RH (2020) Circular RNA: metabolism, functions and interactions with proteins. Mol Cancer 19:172